Evaluation of the Influence of Build and Print Orientations of Unmanned Aerial Vehicle Parts Fabricated Using Fused Deposition Modeling Process

Suraj Ravindrababu[a,b], Yunus Govdeli[a,b], Zhuo Wei Wong[a,b], Erdal Kayacan[c]

[a]*Singapore Center for 3D Printing (SC3DP), Nanyang Technological University, 50 Nanyang Avenue, Singapore 639798, Singapore*
[b]*School of Mechanical and Aerospace Engineering, Nanyang Technological University, 50 Nanyang Avenue, Singapore 639798, Singapore*
[c]*Department of Engineering, Aarhus University, Aarhus 8200, Denmark*

Abstract

The principal objective of this study is to provide an insight into the simulation of fused deposition modeling (FDM) parts considering the influence of build and print orientations. The elastic modulus, strength and Poissons ratio at different build and print orientations are obtained by performing uniaxial tensile tests. Based on the results, an appropriate material model is formed and validated by conducting flexural tests on a flat and curved layer FDM (CLFDM) parts fabricated in various print and build orientations. It is found that the influence of the print orientation or different raster angle is minimal and an averaged isotropic material model can be used to simulate parts in a particular build orientation. The build orientation influences the elastic mechanical response of the flat and CLFDM parts largely. A case study on a flying wing unmanned aerial vehicle (FW-UAV) is presented to analyze the contribution of the build orientation on the strength of the structure. The case study shows that the effect of build orientation in some instances might not be critical and a thorough understanding of the loads interacting with the part is necessary before analyzing the building parameters.

Keywords: Fused deposition modeling, mechanical behaviour, unmanned aerial vehicles, Taguchi and ANOVA analysis, finite element analysis.

1. Introduction

The build and print orientations are essential printing parameters while fabricating functional end-use parts using the fused deposition modeling process (FDM). The FDM technology manufactures parts by extruding semi-molten thermoplastic materials and arranges them in layers. The variation of the manufacturing orientations within the printer volume results in variations in the microstructural design, thus affecting the mechanical behavior of the printed components [1, 2].

Several researchers have studied the effect of print [3, 4, 5, 6, 7] and build orientations [8, 9, 10, 11] on the mechanical capability of FDM parts. Invariably, the researchers conclude that these printing parameters induce anisotropy in the mechanical response on a varying scale depending on the printer type and materials used. Although these results provide an insight into the selection of appropriate printing orientations, it is vital to quantify the difference in stiffness and strength occurring due to different printing orientations, especially for simulating these parts in the pre-design phase. Also, an analysis on the influence of build and print orientations on the mechanical performance of the part is necessary since there are certain advantages of printing in a particular direction. One such example is the ability to print tall structures when the part is oriented in a way that the layers are stacked one above the other. Building in this orientation might be critical in the fabrication of unmanned aerial vehicle (UAV) parts, especially wing sections, since it is structurally beneficial to reduce the number of joints in a component. Hence, it is important for a designer to simulate FDM printed parts to check their mechanical response to an applied load before making plans for 3D printing.

Simulating FDM printed parts using the finite element (FE) method requires a material model which must be robust; and the method adopted in deriving this model has to consider the effect of print and build

Email addresses: suraj001@e.ntu.edu.sg (Suraj Ravindrababu), yunus002@e.ntu.edu.sg (Yunus Govdeli), wong1002@e.ntu.edu.sg (Zhuo Wei Wong), erdal@eng.au.dk (Erdal Kayacan)

orientations. In [12], the FE method is implemented to compare isotropic and anisotropic material models to simulate FDM parts and is concluded that an FDM part must be considered anisotropic. The article that aligns closely to the contributions of this paper is [13], where an orthotropic material model for computing the stiffness matrix to simulate FDM printed polycarbonate parts at various build orientations. It concludes that an isotropic material model is sufficient to simulate FDM parts with different build orientations. The mean values of the elastic mechanical properties in different build directions are given as an input to the FE solver. In addition to the work presented in the aforementioned article, the research in this paper also focusses on investigating the effect of varying raster angles or the print orientations while simulating an FDM printed part. Another closely related study is conducted in [14, 15] on acrylonitrile butadiene styrene (ABS) and ULTEM parts respectively. The article concludes that the arrangement of the layers or the build orientation to the direction of the application of load is critical to the mechanical response of an FDM printed part.

The motivation of this research article arises from the inquisitiveness to analyze the capability of FDM as a manufacturing technology to fabricate UAV components. To reduce the lead time of the UAV, the parts are often arranged or stacked in different directions to maximise the usage of the print volume. In such cases, the build and print orientations of various parts are different, and the designer needs to include their effects in the computational environment to analyze the performance of the component accurately. In this paper, the effects of both print and build orientations on forming an appropriate material model for simulating FDM printed parts are presented. The elastic mechanical properties are obtained through the uniaxial tensile tests. Based on the results of the uniaxial tensile tests, certain assumptions are drawn and validated by conducting simulation on the representative parts. Finally, a strength-based design analysis on a flying wing UAV (FW-UAV) is presented to analyze the criticality of build and print orientations in the fabrication of the structure through the FDM process.

The article comprises of three sections. In Section 2, mechanical characterization of FDM printed parts and the influence of print and build orientations on them is discussed. Also, a valid material model is formulated and validated through the experimental and numerical investigation on flexural tests on flat and CLFDM parts. Section 3 applies the assumptions made for finalising the material model to the FW-UAV structure to determine the contribution of part orientation to the strength of the structure. Taguchi and ANOVA analyses are conducted to accomplish the same and vital conclusions are drawn in Section 4 for simulating FDM printed UAV parts at various print and build orientations.

2. Experimental and Numerical Procedures

The experimental and numerical procedures conducted in this article can be divided into the following parts:

1. **Uniaxial Tensile Tests-Experimentation and Results:** Mechanical characterization of the FDM parts is accomplished by manufacturing them in different build (edge-up (EU),face-up (FU) and straight-up (SU)) and print orientations (0-90°) as shown in Fig. 1. Morphology of the fractured surface is obtained by using scanning electron (SEM) and optical microscopes. The images are studied to understand the influence of print orientation to the elastic modulus and strength of the specimen. The Youngs modulus and the ultimate tensile strength of FDM parts in different build and print orientations are presented and a suitable material model is predicted accounting for the changes in build and print orientations.
2. **Testing of representative samples:** The flexural behavior of flat and curved layer FDM (CLFDM) samples in different build and print orientations is shown. Since the slicing software used for the printer has different travel/toolpath algorithms for flat and curved samples, an additional analysis should be conducted for the curved parts [16, 17, 18]. Geometrical aberrations arising due to the build orientation of a CLFDM sample is analyzed to ensure their influence on the physical response is not profound.
3. **FE simulation of the representative parts:** FE analysis of the flat and CLFDM samples are conducted using the commercial FE package, ABAQUS, and the material model predicted in the previous section is validated.

All parts in this article are fabricated using the Stratasys Dimension Elite FDM printer which has a print volume of 203 x 203 x 305 mm. ABS*plus* is the model material and a polymethyl methacrylate based support material, P400SR, which is soluble in alkaline water is used as the support. The parts are fabricated with a layer thickness of 0.1778 mm and orients it at +45°/-45° to obtain parts with enhanced complex load bearing capability [19]. STL files of the samples are generated using Solidworks ® 2015 CAD package.

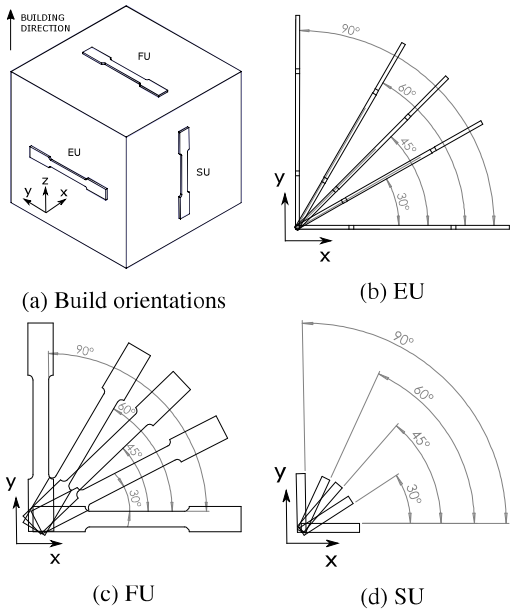

(a) Build orientations (b) EU

(c) FU (d) SU

Figure 1: Tensile specimen oriented in various build and print orientations

2.1. *Uniaxial Tensile Test: Experimentation and Results*

The tensile test samples are prepared according to the ASTM D638-10 Type-1 standard [20]. Five sample are printed for each build and print orientation, amounting to a total of 75 samples. Shimadzu AGX-*plus* desktop testing machine with a load cell capacity of 10 kN is used for performing the tensile tests. The testing system is fitted with TRViewX optical extensometer capable of capturing the axial extension and width in the gauge region of the sample. The tests are performed at a constant displacement rate of 5mm/min. Figure 2 presents the stress-strain trends for FDM printed uniaxial tensile test samples printed in various print and build orientations.

In Fig. 2, the solid lines represent the stress strain behaviour of EU tensile specimens. Similarly, the dashed lines and dash-dot lines represent the behaviour of SU and FU samples, respectively. The plot shows that the EU samples have the highest stiffness and tensile strength as compared to FU and SU oriented samples. Different print orientations are depicted by different colours of the solid, dashed and dash-dot lines. While a variation in stiffness and strength is evident for different build orientations, these parameters are not found to vary across different print orientations. Furthermore, Fig. 2 also showcases the non-linear behavior of tensile

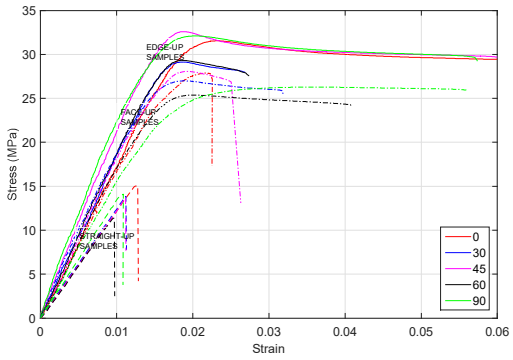

Figure 2: Representative stress-strain plot for flat samples at various print and build orientations.

samples at different print and build orientations. EU and FU samples showed a prominent plastic region, where the material progressively fails through yielding before complete failure while the SU sample fails in a brittle manner. Although the failure mechanism varies across different build orientations, it is found to remain the same for different print orientations.

The rasters inside the FDM part are arranged to reduce the air gap since the print interior style chosen is solid. The rasters are thermoplastic polymers which are in a semi-molten state due to the extrusion process and hence, they result in a phenomenon called as inter-road bonding. The phenomenon is lucidly explained in [21], where an individual raster comes in contact with its neighbours and undergoes necking and consequently, the rasters coalesce at the phase boundary to form a single entity as illustrated in Fig 3a.

Inter-road or inter-raster bonding is critical to understand the mechanics of FDM parts when the raster or print angle within the print bed changes. The bonded area is an essential factor to consider while analyzing the effect of print orientation on the stiffness and strength of an FDM part. Unlike composite materials, where the stress inside the material is induced by the interacting forces between the polymeric matrix and carbon/glass fibre, an FDM printed part comprises of voids instead of the matrix constituent. The load is predominantly carried by the individual rasters and the area of coalescence as shown in Fig. 3b. The effect of the area of coalescence can be further explained by studying the meso-structure of a FU specimen oriented at 45°. The fractured surface is examined under a scanning electron microscope (SEM) to observe the morphology of the surface and the SEM image is given in Fig. 5. From Fig. 5, it can be concluded that the damage initiation happens

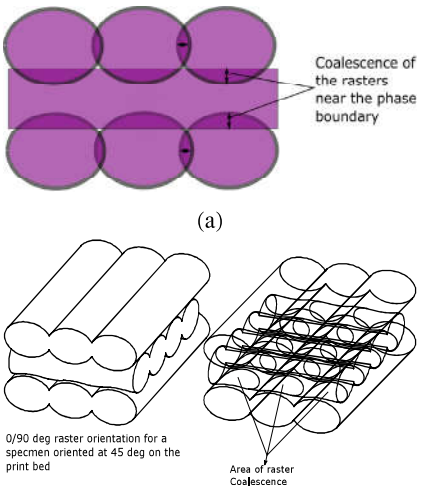

Figure 3: Fig. 3a: Coalescence in the rasters, Fig. 3b: The coalescence area between the rasters which are vital for the performance of the part.

at the inter-facial region between the layers and then advances to the individual rasters. Raster pull out is observed at various regions in the morphology of the fractured surface which shows that the adhesion between the layer fails and the raster is pulled out due to the tensile load. Once the maximum strength of the raster is achieved, they undergo failure in a brittle fashion.

Figure 4 presents the meso-structural arrangements of an EU, FU and SU sample oriented at 0°, 45° and 90° degrees respectively. The density of the meso-structural arrangement is the critical parameter here. The density increases the area of coalescence, which is imperative to the mechanical performance of the FDM part. For EU samples, the meso-structure is more dense compared the other two, resulting in the highest stiffness and strength among all arrangements. Furthermore, FU and SU samples are perceived to have a similar density. However, the pulling direction or the loading direction is different for an SU sample, as seen in Fig. 6.

In the case of the SU sample, the load is applied perpendicular to the direction in which the layers are stacked and hence, owing to the poor adhesion between the layers, the SU sample fails in a fragile manner as shown in Fig. 6 [22]. When the raster orientation changes between the layers, the area of coalescence does not change significantly in the case of an EU and FU sample. Therefore, the contribution to the stress developed in the meso-structure due to varying raster angles is minimal. Since the predominant load bearing element in an SU sample is the adhesive strength between

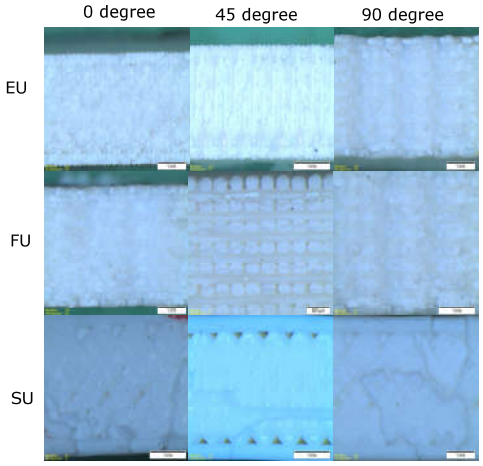

Figure 4: Meso-structure of the fractured surface of EU, FU and SU samples at various print orientations.

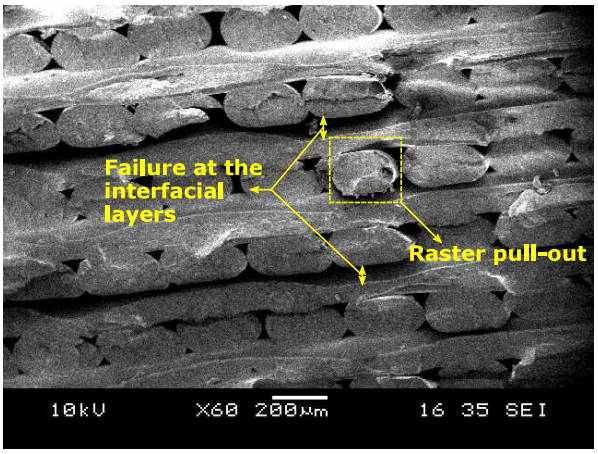

Figure 5: Meso-structure of the fractured surface of an FU oriented FDM part under SEM.

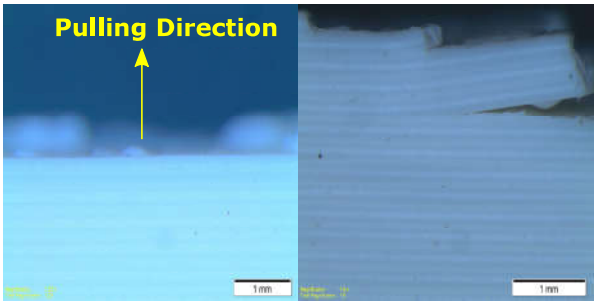

Figure 6: Microscopic image of the fractured edge showing failure between the stacked layers.

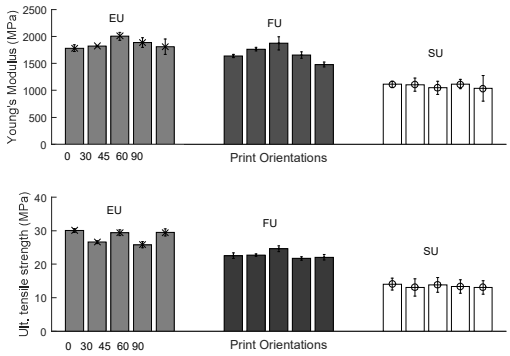

Figure 7: Comparison of the Young's modulus and ultimate tensile strength for various print and build orientations.

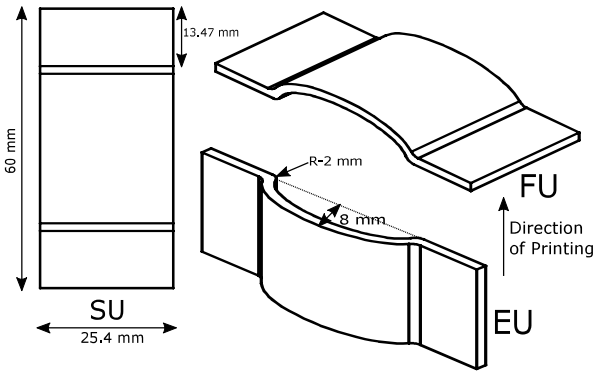

Figure 8: Orientation and dimensions of the curved samples in the build volume.

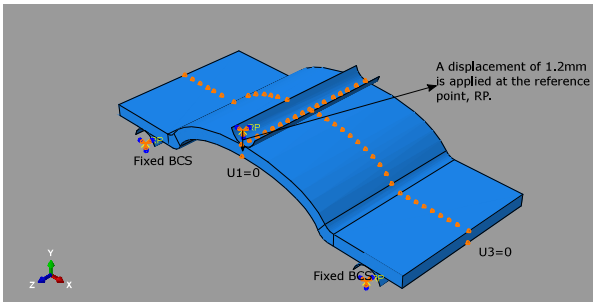

Figure 9: FE model of the CLFDM sample in Abaqus.

the layers, the surface area change in the layers due to the different alignment of the rasters is very unlikely. However, the mechanical properties are predominantly influenced by the alignment of the individual raster to the direction of the load (evident in FU specimens). This influence, although provides a change in the stiffness and strength values, is not alarmingly different from the specimens oriented at other angles as seen in Fig. 7. The standard deviations (SD), marked by the error bars in each print orientation for a build orientation overlap each other and hence, the variation of the stiffness and strength properties along the print orientation is found to be minimal. Therefore for simulating FDM parts fabricated in in different print orientations, the mean of the elastic modulus and the strength value is taken in to consideration at each build orientation as shown in Table 1.

2.2. *Testing and Simulation of Representative Samples: Flexural response of Flat and CLFDM Samples*

The samples used for the three-point bend test for flat samples is prepared according to ASTM D790 standard. Procedure A (small deflection) and Type 1 methods are employed in the experiements. The printed sample has the dimensions 150 x 12.7 x 3.2 mm and a gauge length of 50 mm.Three specimens are printed and tested for each build (EU, FU and SU) and print (0°, 45° and 90°). The cross-head displacement rate (1.3021 mm/min) and the displacement at which the maximum strain in the outer surface reaches a maximum are calculated as per mentioned in the standard. The CLFDM samples are printed in similar print and build orientations as the flat samples. The dimensions of the CLFDM samples are shown in Fig. 8. Both the experiments are conducted using the Instron 5569 testing machine fitted with a load cell capacity of 100 kN.

The experiments focus on studying two critical objectives native to the printing of curved objects/contours. Firstly, the influence of the staircase error, arising due to the slicing options available in the printer interface, on the mechanical behavior of the parts built in different build orientations is studied. Secondly, the effect of varying raster angles or the print orientation of the CLFDM and flat samples is studied.

Linear elastic material properties for different build orientation mentioned in Table 1 is given as the input in the FE solver. The indentors are modelled as rigid bodies using a rigid body constraint option in the software. A linear static analysis is conducted on the samples. A vertical downward displacement of 1.2 is given to the samples where the structure is still elastically deforming. The curved sample is meshed with 26,877 and the flat samples comprises of 96,768 linear hexahedral elements of type C3D8R. The indentors are meshed with quadrilateral elements of type S4R. The FE model of the CLFDM sample in ABAQUS is shown in Fig. 9. FE model of the flat sample is created using a similar approach adopted for modelling CLFDM samples. Hence, the boundary conditions (BCS) and displacement given were similar to that in a CLFDM FE model.

Table 1: Comparison of the Young's modulus, Poisson's ratio and ultimate tensile strength for various build orientations.

Build Orientation	Young's modulus (MPa)			Ultimate tensile strength		Poisson's ratio
	E	SD (± MPa)	% diff (w.r.t SU)	σ_{ult}	SD (± MPa)	
EU	1808.60	88.64	73%	29.50	1.93	0.35
FU	1479.40	147.69	42%	22.06	0.55	0.36
SU	1040.20	48.15	-	11.60	0.97	0.34

Table 2: Comparison of experimental and FE result for the CLFDM samples.

Build Orientation	F/d-Expt (kN/mm)			F/d expt. mean (kN/mm)	F/d-FE (kN/mm)	% diff. of the FE result from the expt.
	0	45	90			
EU	0.018	0.019	0.018	0.0183	0.01875	4%
FU	0.013	0.015	0.013	0.014	0.015	6.7%
SU	0.013	0.013	0.014	0.012	0.013	7.7%

2.3. *Summary of Results of the Analysis on Flat and CLFDM samples*

A quantitative comparison of the elastic mechanical responses of flat and CLFDM samples at different build and print orientations is achieved by calculating the bending stiffness coefficient (F/d) and is listed in Table 2 and 3.

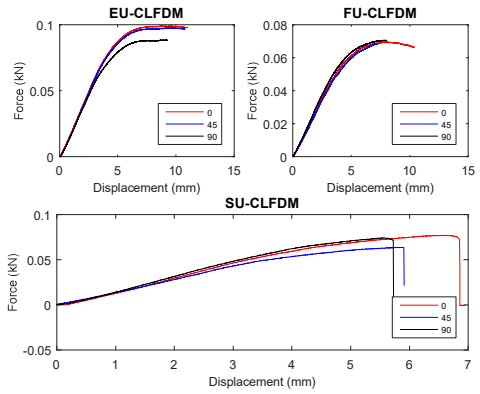

Figure 10: Force versus displacement plot for CLFDM sample in different print and build orientations.

The tables lists the results of the experimental and numerical analysis on flat and CLFDM samples. It is observed that the influence of print orientation on the mechanical performance of these parts is minimal since the variation of F/d is found to be less than 10% which is acceptable since the mechanical responses are influenced by other factors such as raster gap, width and diffusion between rasters. Therefore, an averaged isotropic model is sufficient to simulate the parts with varying raster angles. Moreover, the build orientation has a significant influence on the mechanical performance of these parts. As seen in Table 2 and 3, it is evident that the variation of flexural stiffness coefficient for both the samples is more than 10% for different build orientations. Also, it is observed that a part oriented at 45° provides better stiffness for EU and FU samples as observed in [23] but in SU orientation, the stiffness is minimal, as can be seen in Fig.10 and 11. Unlike FU and SU samples where the arrangement of the rasters and layers contribute to the stiffness, the SU sample's stiffness is dependent on the adhesion between the layers and hence, comparison of the experimental result with FE analysis showed a larger deviation of 7.7% and 11.3% in the case of CLFDM and flat samples. Therefore, it is more favourable to build components oriented in FU and EU direction since they are easier to simulate and there is very less probability for obtaining parts with less discontinuities. Although there are disadvantages, SU orientation provides a critical advantage of building long parts in most of the FDM printers. Therefore, a numerical design analysis shall be done prior to the building of these parts to reveal their stress state.

Table 3: Comparison of experimental and FE result for flat samples.

Build Orientation	F/d-Expt (kN/mm)			F/d expt. mean (kN/mm)	F/d-FE (kN/mm)	% diff. of the FE result from the expt.
	0	45	90			
EU	0.029	0.032	0.031	0.031	0.029	6.4%
FU	0.026	0.028	0.024	0.026	0.025	3.8%
SU	0.023	0.021	0.022	0.022	0.0195	11.3%

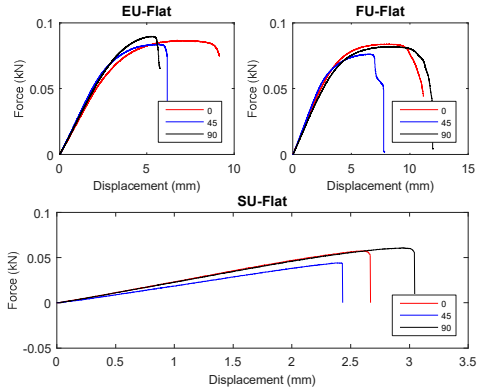

Figure 11: Force versus displacement plot for flat samples at different orientations.

3. Case Study on the Analyses of Build Orientation on the Manufacturing of an FW-UAV

In this section, strength-based structural design based on the FE method is conducted on an FW-UAV planform to demonstrate the numerical analysis that could be performed before deciding the building orientation. The study combines the FE and statistical methods, especially Taguchi and analysis of variance (ANOVA), to determine the contribution of building orientation selection to the mechanical quality of the UAV structure. The approach involves the use of Taguchi method to drastically reduce the number of simulations, therby reducing the lead time in part manufacturing. The ANOVA analysis is performed to study the contribution of build orientation to the UAV's structural integrity. The approach is beneficial since it reduces the prototyping cost in the preliminary structural design phase of the UAV. Also, since they reduce the number of simulations, the computational cost is even less [24, 25].

3.1. Taguchi Method: Factorial Selection and Orthogonal Array Design

The controllable factors chosen for this analysis are the thickness of the skin, number of ribs and the build orientation of the part. The skin thickness is crucial for resisting the buckling loads due to the bending moment. Rib spacing is an essential factor in carrying the aerodynamic loads as well as the shear from the skin panels. The factor values are chosen considering the minimum printable thickness by the printer and the maximum structural weight approximated during the initial design phases. The controllable factors and the levels selected for each of them are listed in Table 4. This section is a comprehensive analysis on the FW-UAV structure, focussing on determining the contribution of build orientation selection to the strength of the structure and design calculations such as the thickness of the skin, rib spacing and spar positions are neglected.

Table 4: Controllable parameters and the levels chosen.

Controllable parameters	Level 1	Level 2	Level 3
Skin thickness	0.5	0.75	1
No. of ribs	9	11	13
Build orientation	EU	FU	SU

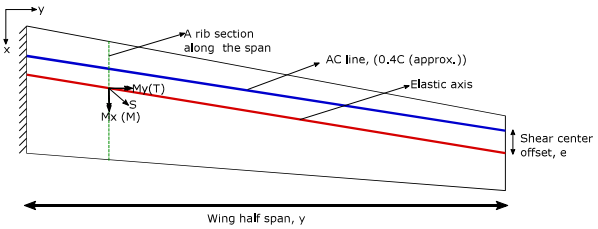

Figure 12: A representative location of elastic axis and cut loads applied along wing span.

Max von-Mises stress and the mass of the structure are considered as the responses from the FE simulation of the UAV structure. The goal of the study is to minimize the von-Mises stress and the weight and hence, the smaller-the-better characteristic is chosen to compute the signal-to-noise ratio (S/N) analysis as shown in (1).

$$S/N = -10.log_{10}[\frac{1}{n}\sum_{i=1}^{n} y_i^2] \quad (1)$$

3.2. FE Model of the FW-UAV

The dynamic responses of the UAV are neglected and a quasi-equilibrium condition is assumed. The loads on the UAV structure is computed for a single maximum load case of 3 which is a safe value to consider as seen in [26]. A factor of safety of 1.5 is included in the calculation of the loads. The aerodynamic loads are computed using an open source solver that uses the vortex lattice method (VLM) to compute the aerodynamic loads. The solver computes the aerodynamic coefficients for the 2D aerofoil profile at various Reynolds number and extrapolates these values onto the 3D analysis. Hence, the effect of thickness/shape of the cross-sections along the wing is taken into consideration [27, 28]. The aerodynamic loads are given in the FE model as cut-loads which comprises of three orthogonal pairs of shear force, bending moment and torsional moments acting on the elastic axis along the span of the UAV, as seen in Fig. 12 [29].

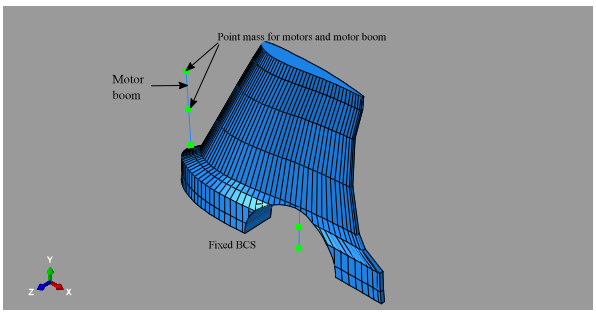

Figure 13: Point mass and BCS in FE model.

Table 5: Number of elements in the final FE model after the mesh convergence test.

Number of ribs	Element type	
	S4R	B31 (158-front, 125-rear)
9	83189	283
11	85071	283
13	85488	283

The shear force, bending moment and the torsional moment is applied using the structural distributing elements which are similar to RBE3 elements [30]. Inertial relief loads, such as the mass of the motors, motor booms, battery etc., are applied as a point mass in the FE model. A fixed BCS is employed at the plane of the symmetry of the model as the wing is approximated as cantilever beam fixed to the mid-rib. The mechanical properties from Table 1 are used as an input to the software. The FE model created in ABAQUS is shown in Fig. 13. The skin and the ribs are meshed with a 4-node shell element, S4R, and the motor booms are meshed using the two node linear beam element, B31. Three FE models are created with varying number of ribs depending upon the combinations mentioned in the L9 orthogonal array. The number of elements created for each FE model afer the mesh sensitivity analysis is shown in Table 5.

The combination of the controllable factors in each simulation, the maximum von-Mises stress and the structural weight of each configuration is recorded in Table 6. The Taguchi method based on the L9 orthogonal array is conducted to provide a simple, computationally cost-effective and a systematic method for determining the optimum level of the controllable factors. The S/N ratio for both the responses is recorded in Table 7 and 8.

Table 7: S/N response table for von Mises stress (MPa).

Levels	Skin thickness	No. of Ribs	Build Orientation
1	-19.61	**-14.40**	-15.48
2	-15.49	-15.71	**-15.36**
3	**-11.32**	-16.31	-15.58
Delta	8.29	1.91	0.22
Rank	1	2	3

Table 8: S/N response table for structural mass (kg).

Levels	Skin thickness	No. of Ribs	Build Orientation
1	**-0.11787**	**0.04140**	**-0.95074**
2	-1.01725	-0.95630	-0.95844
3	-1.83405	-2.05427	-1.05999
Delta	1.71617	2.09567	0.10926
Rank	2	1	3

The highlighted values in the tables show the optimum values that could be chosen for the least weight and best mechanical performance of the UAV. A low stressed structure is possible if the skin thickness, the number of ribs and the build orientation are to be 1 mm, 9 and FU respectively. For the least structural mass, these factors must take the values of 0.5 mm, nine ribs and EU orientation. Without exception, both the responses demand a maximum rib quantity of 9. Therefore in Table 6, between analyses 1 and 4, the configuration for analysis 4 is the least stressed among the two and the structural mass (0.999 kg) is close to the mass value given as the input during the stability and aerodynamic analyses. Therefore, the factors defined in analysis 4 can be chosen as the most optimum combination for the fabrication of the initial prototype.

3.3. ANOVA Analysis

An ANOVA analysis is conducted to examine the influence of build orientation on the mechanical behavior of the UAV configuration. ANOVA is a statistical method which is used to determine the individual interactions of the controllable factors towards the recorded responses. It is used to study the effect of the skin thickness, the number of ribs and the build orientation on the maximum von Mises stress and the mass (conducted to obtain a direction for further structural optimisation) of the structure. This analysis is carried out at a 5% significance level and a 95% confidence level. The results of ANOVA on the von Mises stress and the mass of the structure is shown in Table 9.

The results of the ANOVA analysis is critical in understanding the contribution of each control factor to the

Table 6: The L9 orthogonal array, response values from FE simulations and the S/N values for the responses recorded.

Analysis no.	Sheet thickness	No. of ribs	Build Orientation	von Mises (MPa)	Mass (kg)	S/N von Mises	S/N Mass
1	**0.5**	**9**	**EU**	**8.342**	**0.889**	**-18.425**	**1.022**
2	0.5	11	FU	9.742	1.010	-19.773	-0.086
3	0.5	13	SU	10.760	1.160	-20.636	-1.289
4	**0.75**	**9**	**FU**	**5.239**	**0.999**	**-14.385**	**0.009**
5	0.75	11	SU	6.100	1.120	-15.707	-0.984
6	0.75	13	EU	6.592	1.270	-16.380	-2.076
7	**1**	**9**	**SU**	**3.310**	**1.110**	**-10.397**	**-0.906**
8	1	11	EU	3.820	1.230	-11.641	-1.789
9	1	13	FU	3.944	1.380	-11.919	-2.798

Table 9: Results of ANOVA on the von Mises stress and structural mass of the UAV configuration.

Source	DF	SS	Mean square (MS)	% contribution
von Mises stress				
Skin	2	**53.5428**	**26.7714**	**93%**
No of ribs	2	3.3058	1.6529	6%
Build orientation	2	0.3983	0.1991	0.7%
Error	2	0.4074	0.2037	
Total	8	57.6543		
Structural mass				
Skin	2	0.07282	0.03641	39.8%
No of ribs	2	**0.110321**	**0.05516**	**60.2%**
Total	8	0.183142		

maximum von Mises stress of the UAV structure. The significance of these factors is determined by comparing the F-values of each control factor. From Table. 9, the skin thickness of the structure is the factor affecting the stresses developed in the structure (93%). For this particular configuration, the build orientation of the structure did not influence its mechanical performance. Also, the mass of the structure is found to be primarily affected by the number of ribs (60.2%) rather than the thickness of skin (39.8%) whose surface is larger than that of the rib sections. Nevertheless, these results provide insight into the most critical factors, the maximum von Mises stress and structural mass, affecting the two essential responses that are considered in the preliminary design phase.

4. Conclusion

The build orientation has a larger impact than print orientation on the elastic deformation of an FDM printed part. While printing parts using FDM, they should be oriented in such a way that the layers with the longest contours are aligned with the direction of the applied tensile load. Layer arrangement perpendicular to the direction of the applied load generated very poor results. For simulating parts which are oriented at different angles in the print bed, an averaged isotropic model can be used. A similar approximation could not be made for simulating parts with different build orientation since the difference in the flexural stiffness coefficient (F/d) within the elastic region is found to be more than 10%. However, beyond the yield strength, it becomes critical to choose both the print and build orientation since the non-linear behaviour is highly dependent on the meso-structural design.

Once the loads acting on a component are determined, a simple FE simulation could be performed using the mechanical properties obtained in the three build orientations to determine the maximum stress in the component. If the maximum stresses are within the yield strength of a particular build orientation, the effect of printing parameters can be neglected. The mechanical properties mentioned in this article are native to the type of printer, nozzle diameter and the layer height of the printing process. Hence, it is essential to characterize the mechanical properties of the parts printed with a particular printer before attempting to fabricate functional parts.

5. Conflict of interest

None declared.

6. Acknowledgements

This research is supported by the National Research Foundation, Prime Ministers Office, Singapore under its Medium-Sized Centre funding scheme.

References

[1] K. Chin Ang, K. Fai Leong, C. Kai Chua, M. Chandrasekaran, Investigation of the mechanical properties and porosity relationships in fused deposition modelling-fabricated porous structures, Rapid Prototyping Journal 12 (2) (2006) 100–105.

[2] C. Majewski, N. Hopkinson, Effect of section thickness and build orientation on tensile properties and material characteristics of laser sintered nylon-12 parts, Rapid Prototyping Journal 17 (3) (2011) 176–180.
[3] W. Wu, P. Geng, G. Li, D. Zhao, H. Zhang, J. Zhao, Influence of layer thickness and raster angle on the mechanical properties of 3d-printed peek and a comparative mechanical study between peek and abs, Materials 8 (9) (2015) 5834–5846.
[4] B. Rankouhi, S. Javadpour, F. Delfanian, T. Letcher, Failure analysis and mechanical characterization of 3d printed abs with respect to layer thickness and orientation, Journal of Failure Analysis and Prevention 16 (3) (2016) 467–481.
[5] I. Durgun, R. Ertan, Experimental investigation of fdm process for improvement of mechanical properties and production cost, Rapid Prototyping Journal 20 (3) (2014) 228–235.
[6] O. Carneiro, A. Silva, R. Gomes, Fused deposition modeling with polypropylene, Materials & Design 83 (2015) 768–776.
[7] A. K. Sood, R. K. Ohdar, S. S. Mahapatra, Parametric appraisal of mechanical property of fused deposition modelling processed parts, Materials & Design 31 (1) (2010) 287–295.
[8] F. Xu, H. Loh, Y. Wong, Considerations and selection of optimal orientation for different rapid prototyping systems, Rapid Prototyping Journal 5 (2) (1999) 54–60.
[9] M. Uddin, M. Sidek, M. Faizal, R. Ghomashchi, A. Pramanik, Evaluating mechanical properties and failure mechanisms of fused deposition modeling acrylonitrile butadiene styrene parts, Journal of Manufacturing Science and Engineering 139 (8) (2017) 081018.
[10] W. C. Smith, R. W. Dean, Structural characteristics of fused deposition modeling polycarbonate material, Polymer testing 32 (8) (2013) 1306–1312.
[11] K. P. Motaparti, G. Taylor, M. C. Leu, K. Chandrashekhara, J. Castle, M. Matlack, Experimental investigation of effects of build parameters on flexural properties in fused deposition modelling parts, Virtual and Physical Prototyping (2017) 1–14.
[12] A. Bellini, S. Güçeri, Mechanical characterization of parts fabricated using fused deposition modeling, Rapid Prototyping Journal 9 (4) (2003) 252–264.
[13] M. Domingo-Espin, J. M. Puigoriol-Forcada, A.-A. Garcia-Granada, J. Lluma, S. Borros, G. Reyes, Mechanical property characterization and simulation of fused deposition modeling polycarbonate parts, Materials & Design 83 (2015) 670–677.
[14] R. H. Hambali, H. Celik, P. Smith, A. Rennie, M. Ucar, Effect of build orientation on fdm parts: a case study for validation of deformation behaviour by fea, in: IN: Proceedings of iDECON 2010international conference on design and concurrent engineering, Universiti Teknikal Malaysia Melaka, Melaka, 2010, pp. 224–228.
[15] A. S. El-Gizawy, S. Corl, B. Graybill, Process-induced properties of fdm products, in: Proceedings of the ICMET, International Conference on Mechanical Engineerings and Technology Congress & Exposition, 2011.
[16] S. Singamneni, A. Roychoudhury, O. Diegel, B. Huang, Modeling and evaluation of curved layer fused deposition, Journal of Materials Processing Technology 212 (1) (2012) 27–35.
[17] B. Huang, S. Singamneni, Curved layer fused deposition modeling with varying raster orientations, in: Applied Mechanics and Materials, Vol. 446, Trans Tech Publ, 2014, pp. 263–269.
[18] D. Adams, C. Turner, An implicit slicing method for additive manufacturing processes, Virtual and Physical Prototyping (2017) 1–6.
[19] A. K. Sood, R. K. Ohdar, S. S. Mahapatra, Parametric appraisal of mechanical property of fused deposition modelling processed parts, Materials & Design 31 (1) (2010) 287–295.
[20] W. C. Smith, R. W. Dean, Structural characteristics of fused deposition modeling polycarbonate material, Polymer testing 32 (8) (2013) 1306–1312.
[21] B. Huang, S. Singamneni, Raster angle mechanics in fused deposition modelling, Journal of Composite Materials 49 (3) (2015) 363–383.
[22] J. Du, Z. Wei, X. Wang, J. Wang, Z. Chen, An improved fused deposition modeling process for forming large-size thin-walled parts, Journal of Materials Processing Technology 234 (2016) 332–341.
[23] M. Dawoud, I. Taha, S. J. Ebeid, Mechanical behaviour of abs: An experimental study using fdm and injection moulding techniques, Journal of Manufacturing Processes 21 (2016) 39–45.
[24] C.-L. Lin, J.-H. Yu, H.-L. Liu, C.-H. Lin, Y.-S. Lin, Evaluation of contributions of orthodontic mini-screw design factors based on fe analysis and the taguchi method, Journal of biomechanics 43 (11) (2010) 2174–2181.
[25] T. Kıvak, Optimization of surface roughness and flank wear using the taguchi method in milling of hadfield steel with pvd and cvd coated inserts, Measurement 50 (2014) 19–28.
[26] D. Locascio, C. Ramee, E. Schaus, K. D. Cooksey, E. Spero, D. N. Mavris, A framework for integrated analysis, design, and rapid prototyping of small unmanned airplanes, in: 16th AIAA Aviation Technology, Integration, and Operations Conference, 2016, p. 3447.
[27] S. Rajagopal, R. Ganguli, Multidisciplinary design optimization of a uav wing using kriging based multi-objective genetic algorithm, AIAA Paper 2219 (2009) 2009.
[28] U. Ozdemir, Y. O. Aktas, A. Vuruskan, Y. Dereli, A. F. Tarhan, K. Demirbag, A. Erdem, G. D. Kalaycioglu, I. Ozkol, G. Inalhan, Design of a commercial hybrid vtol uav system, Journal of Intelligent & Robotic Systems 74 (1-2) (2014) 371–393.
[29] F. Hürlimann, R. Kelm, M. Dugas, G. Kress, Investigation of local load introduction methods in aircraft pre-design, Aerospace Science and Technology 21 (1) (2012) 31–40.
[30] D. Systèmes, Abaqus analysis users manual, Simulia Corp. Providence, RI, USA.